

# An Agile, Portable Antenna System for LEO Megaconstellation-Based PNT

Wenkai Qin<sup>\*</sup>, Zacharias M. Komodromos<sup>†</sup>, Todd E. Humphreys<sup>\*</sup>

<sup>\*</sup>*Department of Aerospace Engineering and Engineering Mechanics, The University of Texas at Austin*

<sup>†</sup>*Department of Electrical and Computer Engineering, The University of Texas at Austin*

## ABSTRACT

This paper develops an antenna system to support use of signals from low Earth orbit (LEO) megaconstellations to conduct satellite beam and channel occupancy studies. The antenna system is based on an articulated horn antenna that can reposition itself from one LEO satellite vehicle (SV) to another in less than a second, which allows quasi-continuous LEO signal tracking despite the frequent satellite handoffs that occur in a LEO-based communications network. It offers an alternative to phased-array antennas for LEO megaconstellation signals, which are not yet commercially available at a reasonable cost. The system automatically directs its horn antenna towards transmitting LEO SVs such that acquisition and tracking through a matched filter can be performed using known portions of the signal structure. This system serves as a proof-of-concept and development base for a full LEO position, navigation, and timing (PNT) solution. Experimental results are presented showing successful sequential acquisition of time of arrival measurements from SpaceX's Starlink constellation as well as preliminary results for beam and channel occupancy, observing that up to three SVs may be simultaneously transmitting assigned beams toward a given user service cell.

## I. BIOGRAPHIES

Wenkai Qin (B.S., Harvey Mudd College) is a Ph.D. student in the Department of Aerospace Engineering and Engineering Mechanics at The University of Texas at Austin and a graduate research assistant in the UT Radionavigation Laboratory. His current research interests include LEO PNT, swarm-based navigation, and SLAM.

Zacharias M. Komodromos (B.S., Iowa State University) is a Ph.D. student in the Department of Electrical and Computer Engineering at The University of Texas at Austin and a member of the UT Radionavigation Laboratory. His research interests include wireless communications and re-purposing broadband Internet satellites for positioning, navigation, and timing.

Todd E. Humphreys (B.S., M.S., Utah State University; Ph.D., Cornell University) holds the Ashley H. Priddy Centennial Professorship in Engineering in the Department of Aerospace Engineering and Engineering Mechanics at the University of Texas at Austin. He is Director of the Wireless Networking and Communications Group and of the UT Radionavigation Laboratory, where he specializes in the application of optimal detection and estimation techniques to positioning, navigation, and timing. His awards include the UT Regents' Outstanding Teaching Award (2012), the NSF CAREER Award (2015), the ION Thurlow Award (2015), the PECASE (NSF, 2019), and the ION Kepler Award (2023). He is Fellow of the Institute of Navigation and of the Royal Institute of Navigation.

## II. INTRODUCTION

Recent research has shown increased interest in using low Earth orbit (LEO) satellite constellations as a means to obtain position, navigation, and timing (PNT) solutions. As noted in [Humphreys, 2017], [Dolman, 2012], [Iannucci and Humphreys, 2022], LEO PNT offers improved robustness and redundancy against jamming and anti-satellite warfare, as well as more precise positioning when compared to traditional MEO approaches. As no such dedicated LEO PNT constellation exists yet, researchers have instead begun to opportunistically exploit commercial LEO communications. For instance, recent work has already demonstrated the feasibility of Doppler-based positioning based on observations of signals sent by Starlink's constellation of over 3,000 LEO satellites [Neinavaie et al., 2022]. However, despite its relative merits over Doppler-based positioning in terms of accuracy and time-to-fix, opportunistic pseudorange-based PNT remains an unproven solution. For instance, consider that the 240 MHz per-channel Starlink bandwidth possibly offers nanosecond-accurate timing, an improvement upon the 15 ms accuracy offered by Doppler-based positioning [Psiaki, 2021], [Humphreys et al., 2023], [Neinavaie et al., 2022].

It is well-known that the accuracy of pseudorange-based PNT improves with the reduction in the dilution of precision [Teng and Wang, 2016]. Generally speaking, as the number of available pseudorange measurements to unique SVs increases, so

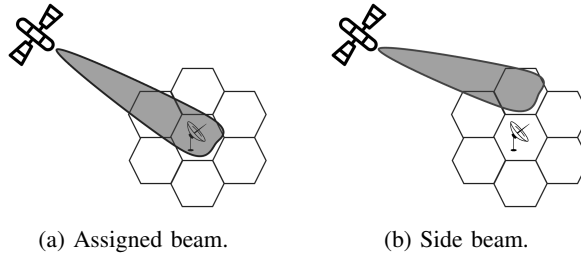


Fig. 1: Illustrated example of assigned and side beams. In each subfigure, the hexagonal grid represents a distribution of service cells on the ground. The antenna in the center represents an opportunistic receiver. If the SV transmits to the service cell occupied by the receiver, as is shown on the left, then we refer to the beam as an assigned beam. If the SV transmits to any other service cell, such as the neighboring service cell as shown on the right, then we refer to the beam as a side beam.

too does the estimation problem’s geometric strength, in turn enabling a more accurate PNT solution. Minimally, if  $d$  is the number of physical dimensions under consideration, including time,  $n \geq d$  pseudorange measurements are required to obtain an observable set of coordinates. Yet multiple simultaneous pseudorange measurements using signals of opportunity has yet to be shown, partly due to the unique challenges encountered when non-cooperatively acquiring LEO communications signals.

These challenges are as follows: First, unlike traditional GNSS satellites that use publicly-known sequences to aid signal acquisition and tracking, LEO communications megaconstellations typically employ proprietary signal structures known only to the companies designing them. In fact, Starlink’s basic signal structure was only recently unveiled, with significant work still remaining regarding additional exploitable signal features and signal timing [Humphreys et al., 2023]. As such, despite LEO satellites enjoying signal-to-noise ratios (SNR) that can be 30 dB higher than those of traditional GNSS satellites [Nardin et al., 2020], signal acquisition remains difficult without pointing directly at an SV that is also directly transmitting to the receiver’s location. Second, efficient operation of a satellite communications constellation dictates that each SV beamforms to cover a particular region on the ground, known as a service cell. The particular service cell that is covered hypothetically changes with user demand and SV movement as the SV passes over user terminals, among other factors. Consequently, from a non-cooperating receiver’s perspective, it becomes difficult to uniquely determine which satellite(s) are beamforming towards the receiver, from the set of SVs passing overhead at any given time. Third, the fact that LEO satellites occupy orbits with altitudes much closer than those of traditional GNSS satellite constellations ( $\sim 550$  vs.  $\sim 20,200$  km) means faster dynamics and a higher Doppler effect. In turn, the signal acquisition and lock problems become more challenging.

A simple alternative to receiver beamforming would be to employ signal processing techniques to acquire multiple low-SNR signals with a rigidly-affixed antenna, in the style of traditional GNSS signal tracking. However, the predictable portion of the Starlink frame signal is currently limited to a small fraction of each frame, requiring a received SNR of at least -15 dB [Komodromos et al., 2023]. As such, the system described in this paper points the antenna to relax the requirement on known signal proportion, and leaves a mechanically simpler system for later development.

As SpaceX’s Starlink megaconstellation currently boasts the most mature deployment amongst LEO broadband communications networks, a single receiver often has simultaneous line-of-sight access to multiple Starlink SVs. Thus, the Starlink constellation offers the best target for testing a rapid-switching antenna pointing system.

This paper’s approach uses a dual-axis mount to focus an attached antenna on a Starlink SV passing overhead. With a matched filter, downstream signal processing performs acquisition of the received transmission using the predictable portion of the signal structure, as known from [Humphreys et al., 2023], and extracts a time of arrival (TOA) measurement.

## A. Terminology

It will be useful to define several new terms related to opportunistic use of broadband LEO signals for PNT. As described in [Iannucci and Humphreys, 2022] and [Humphreys et al., 2023], Starlink Ku-band downlink signals are sent via directional beams from overhead satellites on one of eight 240-MHz channels. Similarly, OneWeb signals are sent via beam-channel combinations [Blázquez-García et al., ].

**Assigned beam:** Beam directed by an SV toward the service cell in which the user’s receiver is located.

**Side beam:** Beam directed by an SV toward a service cell other than the one in which the user’s receiver is located. Side-beam signals received by the user’s receiver will be weaker than assigned-beam signals, but they may still be powerful enough to obtain accurate TOA measurements.

**Assigned channel:** Channel corresponding to an assigned beam.

**Side channel:** Channel corresponding to a side beam.

**Assignment triad:** A unique SV-beam-channel assignment to a particular service cell.

**Fixed assignment interval:** Interval of time over which beam-channel assignments remain fixed across the constellation.

## B. Open Questions

In this and follow-on papers, we seek to answer the open questions posed below. Answers to these questions will bring opportunistic pseudorange-based LEO PNT closer to practice.

- 1) From how many unique SVs, on average, can a user receive assigned or side beams strong enough for accurate TOA measurements? As mentioned above, the greater the geometric diversity of transmitters participating in a PNT solution, the more accurate the solution.
- 2) Is there a simple pattern that can be used to predict assignment triads? If so, then less dwell and switching time may be spent pursuing SVs whose transmissions are not detectable, allowing for a higher density of acquired satellites per unit time.
- 3) What is the range of absolute received power into a hemispherical antenna for an assigned or side beam? If we have some knowledge of the absolute power we can expect to receive, that it becomes possible to know whether or not we will receive the required SNR into an antenna with arbitrary gain.

## C. Contributions

This paper makes three contributions. First, it provides a selection of known Starlink constellation quantities and qualities to inform platform design and experimental methodology. Second, it presents the new capture platform in terms of its hardware and software, before detailing data capture methods employed for the purpose of this study. Finally, it presents new results obtained with the proposed platform.

# III. STARLINK CHARACTERISTICS

In support of the platform design and open questions discussed in the remainder of this paper, this section details various pertinent quantities and qualities of the Starlink constellation. It first focuses on important parameters and features of the Starlink signal structure, then introduces some new terminology to describe useful transmission patterns of the Starlink constellation.

## A. Signal Structure

This paper adopts the terminology and Starlink-specific parameters as presented in [Humphreys et al., 2023]. For convenience, we provide a brief summary of the important signal properties.

As shown in Fig. 2, each Starlink frame consists of 302 non-zero intervals of equal duration and one empty frame guard interval, all sent sequentially in time. A single full Starlink frame length takes  $T_f = 1/750$  s to send. While the first interval contains a time-domain sequence, all the following intervals contain OFDM symbols with  $N = 1024$  orthogonal subcarriers per symbol. The first two intervals are common to all frames sent by all SVs, referred to as the primary and secondary synchronization sequences (PSS and SSS, respectively). These known sequences can be generated according to [Humphreys et al., 2023]. The OFDM subcarriers collectively occupy a channel bandwidth of 240 MHz; Starlink has eight such channels laid out across the 10.7-12.7 GHz frequency band. It should be noted that the first two channels are yet unused.

These synchronization sequences are remarkable: similar to how a traditional GNSS receiver uses civil spreading codes, an opportunistic receiver can use the PSS and SSS to construct a local replica. Correlation against such a local replica yields TOA and Doppler measurements, the building blocks of PNT.

## B. Beamforming Overview

As mentioned in Section I, opportunistic use of Starlink signals carries a particular set of challenges when attempting to uniquely determine which satellites are transmitting to a given user service cell. Although dozens of satellites might be passing overhead at any time and each satellite can form up to 48 Ku-band downlink beams [Blázquez-García et al., ], [Yang and Soloviev, 2023], any given service cell may only be targeted by one or two satellites [Iannucci and Humphreys, 2022]. Limitation to these few satellites causes the PNT problem geometry to become poor or even underdetermined. If possible, the ability to also

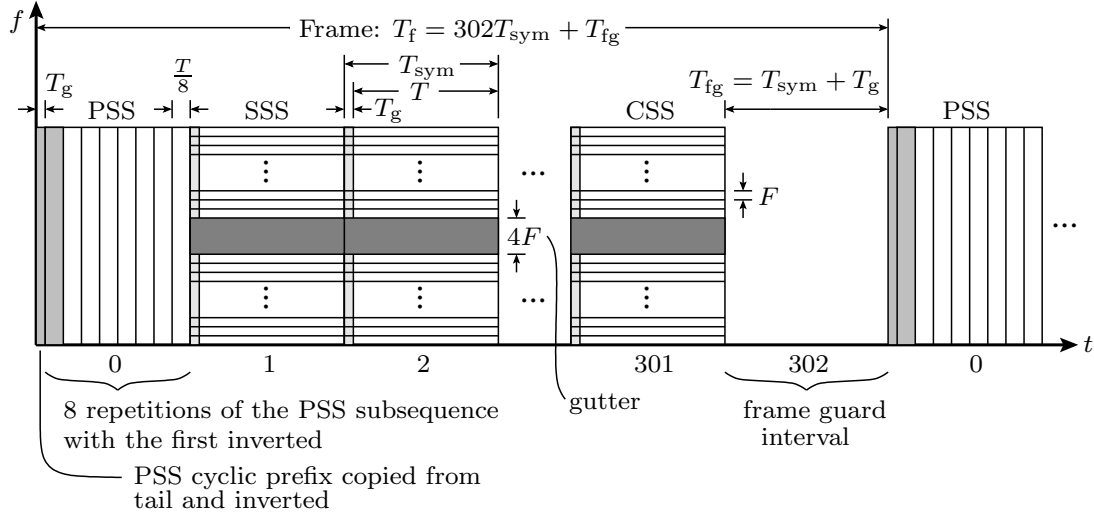


Fig. 2: Starlink frame structure along time-frequency dimensions for a single channel (from [Humphreys et al., 2023]). The first two intervals are occupied by the time-domain PSS and OFDM symbol SSS. All following nonzero intervals also contain OFDM symbols, each one supported by 1024 orthogonal subcarriers. The channel bandwidth is 240 MHz, and frames are sent at 750 Hz, including the frame guard.

acquire pseudoranges from SVs from outside this set could greatly increase the degree of multilateration, thereby recovering PNT accuracy.

Possibly, the use of known sequences as described in Section III to exploit signals destined for neighboring service cells could aid in this regard. Public filings such as [SpaceX, 2019] indicate the Starlink network transmits to individual hexagonal service cells about 20 km wide; however, the transmitted power does not necessarily fall sharply to 0 at service cell edges, especially when the satellite is far from the nadir position. This possibility is supported by an example cross-correlation with the combined PSS and SSS, as presented in Fig. 3.

We introduce the following terminology for the remainder of this paper. First, we use the term "assigned beam" to describe any beam primarily directed at the service cell in which a given receiver resides. These beams tend to possess stronger SNR and often have observable power signatures with little to no signal processing required. Any of the eight Starlink channels that the beam occupies will be referred to as "assigned channels." In contrast, "side beams" are designated as any beams that are not pointed to the occupied service cell. These beams tend to be weaker than assigned beams, but their transmissions can sometimes be used for pseudorange measurements after correlation with a local replica. Accordingly, "side channels" represent any channels via which a given beam occupies.

To facilitate efficient data transmission to and from Starlink users, one can expect that beam and channel assignments change as the transmitting satellites pass overhead. To an opportunistic receiver, the expected assignment state after a change is not predictable; yet, the timing of the change is.

Observations made over the past year indicate that any beam and channel switching occurs at regular, predictable intervals. Beginning with the GPS second reset per week, all beam and channel switching occurs every 15 GPS seconds. To be clear, an assignment change is not guaranteed at every 15-second increment, but if one does occur, it will be on said increment. It then follows that no changes will occur within the 15-second interval between increments. As such, the 15-second intervals will be referred to in this paper as "fixed assignment intervals."

#### IV. SIGNAL CAPTURE PLATFORM

This section introduces the agile antenna system developed over the past several months for the purpose of this and future studies. It begins with a description of the hardware and provides major physical parameters considered in the mechanical design. It then details the software front-end and back-end.

##### A. Hardware

We used an Interbotix WidowX Dual XM430 pan-tilt mount as the assembly actuator. A picture of the device is shown in Fig. 4(a). Three Dynamixel XM430 DC motors collectively move the turret - while only one motor is responsible for azimuth

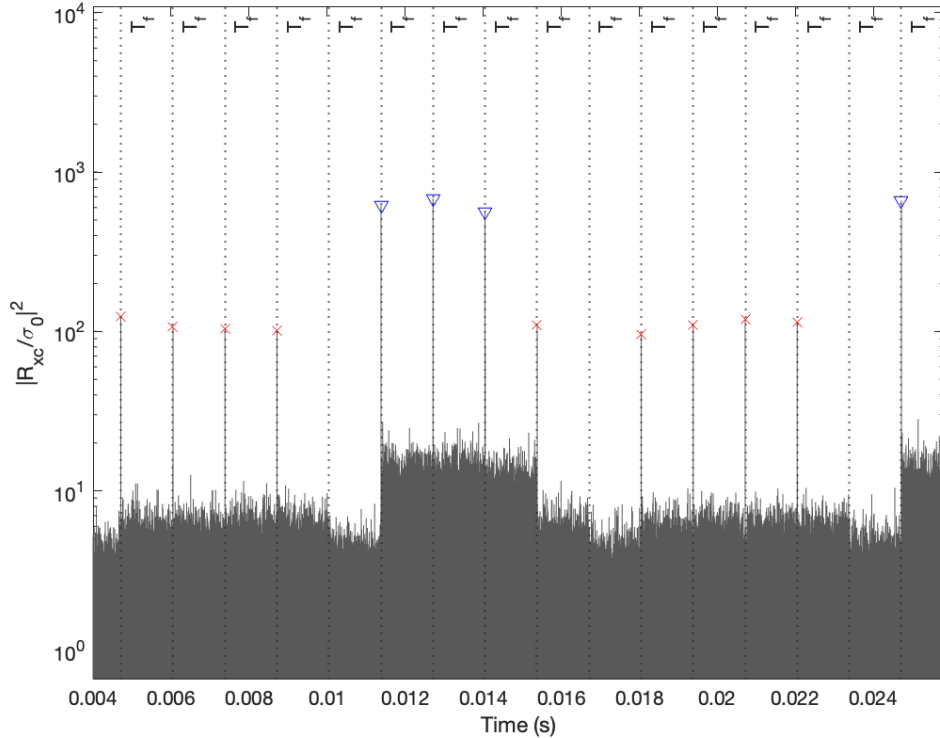


Fig. 3: Noise-scaled cross-correlation of a captured Starlink signal against a local replica consisting of PSS and SSS. Blue triangles denote strong peaks indicating receipt of Starlink frames sent via an assigned beam; red crosses denote relatively weaker peaks from a side beam. Frame intervals are denoted with vertical dotted lines labelled  $T_f$ , indicating that peaks occur at regular intervals, with minor deviations.

movement, two are responsible for elevation movement. Each motor has a stall torque of 4.10 Nm and a no-load speed of 276 deg/s, and both of the elevation motors were required for stall-free actuation of the mounted feedhorn [Robotics, 2023]. The system receives using an NSI-MI manufactured standard gain pyramidal feedhorn fixed atop the pan-tilt turret with 80/20 T-slot aluminum prototyping material. The antenna weighed 1.2 kg, had a 24.4 dBi nominal gain, and was tuned to the frequency range 10.0-15.0 GHz, which covered the Starlink allotted frequency bands of 10.7-12.7 GHz [Humphreys et al., 2023], [Neinavaie et al., 2021], [NSI-MI, 2023]. Again using 80/20 aluminum prototyping stock, we also constructed a wide base under the turret for stabilization under rapid switching from satellite to satellite. To maintain kinematic range of motion, the base was constructed with sufficient height to ensure the extremities of the low-noise block attached to the feedhorn would not collide with the ground in any orientation. To increase the maximum pointing elevation, the pan-tilt turret was cut and remounted onto the assembly base such that it no longer lay in the path of the low-noise block as the antenna precessed relative to the base.

The main advantage of the current capture equipment when compared to those used for [Humphreys et al., 2023] was its switching time. Whereas previous equipment often took up to 30 seconds to change observed satellites, the current antenna consistently switches in less than a second. This allowed for more satellites to be observed in a short period of time. Further, the antenna continuously tracks observed satellites with errors consistently less than 1 degree, even when satellites passing close to zenith (i.e. elevations close to 90 degrees) demanded relatively high azimuth rates.

Fig. 6 illustrates the capture equipment used, which is largely unaltered from that used in [Humphreys et al., 2023]. The pyramidal feedhorn first feeds signals to a low-noise block with a conversion gain of 60 dB and a noise figure of 0.8 dB [EverythingRF, 2023].

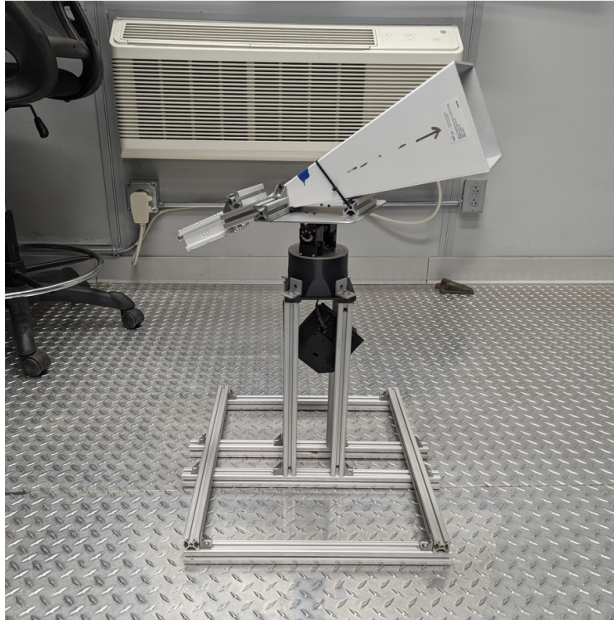
There are two main capture modes available: a narrowband mode and a wideband mode. The narrowband mode offers data at a 16-bit complex sampling, but can only capture at 62.5 Msps. Conversely, the wideband mode does not offer extended data capture, but does allow a live spectrogram view that covers a total bandwidth of just greater than 1 GHz, a useful feature for making power-based observations of channel occupancy.



(a) Interbotix WidowX Dual XM430 Pan & Tilt Turret.



(b) NSI-MI Standard Gain Horn Antenna ANT-SGH.



(c) Assembled directed antenna system.

Fig. 4: Physical hardware components used to construct the receiver assembly.

## B. Software

The software consists of two major modules: a trajectory manager and a motor controller as shown in Fig. 6. The modules run mutually asynchronously and communicate via shared storage. This section will present these modules separately.

The trajectory manager has several jobs. It (1) propagates orbits, (2) processes user inputs, (3) presents a graphical interface, (4) runs a targeting protocol, and (5) submits trajectories produced to the motor controller.

The trajectory manager first downloads all Starlink two-line elements (TLEs) from CelesTrak NORAD automatically on a daily basis, and then propagates the TLEs using an SGP4 simplified perturbation model. This industry-standard propagation technique has an error of approximately 1 km at epoch and grows between 1 and 3 km a day [Vallado et al., 2006]. Though this simplified model does not provide trajectories with errors small enough for PNT, this does not prevent tracking of a satellite using a directed antenna receiver. Under worst-case scenarios, the approximate upper bound on the tracking error due to orbit propagation is at most  $\sim 0.42$  degrees. This orbital propagation error is tolerable as the feedhorn has a beamwidth on the order of several degrees and the Dynamixel motor has a 0.25-degree backlash [Robotis, 2023].

The trajectory manager employs a Python module called curses to drive the text-based user interface (TUI) and input handling. When compared to full graphical user interfaces (GUIs) such as PyQt, TUIs prove to be lightweight, easily adaptable, and quickly reconfigurable, all favorable qualities for rapid prototyping and automation. In our implementation, this allowed our combined propagation and interface loop to run consistently at 20 Hz, enabling live status updates and rapid actuator response to user commands. Fig. 7 presents a screenshot of the user interface and introduces the major interface components. The quick access list of keyboard commands at the TUI's bottom is not pictured. Several important hotkeys initiate a tracking quickchange, toggle the autotargeting mode, and save the current configuration to storage. Section IV-B discusses the specifics of the autotargeting algorithm. Ultimately, whether in automatic or manual targeting mode, the interface selects a satellite to

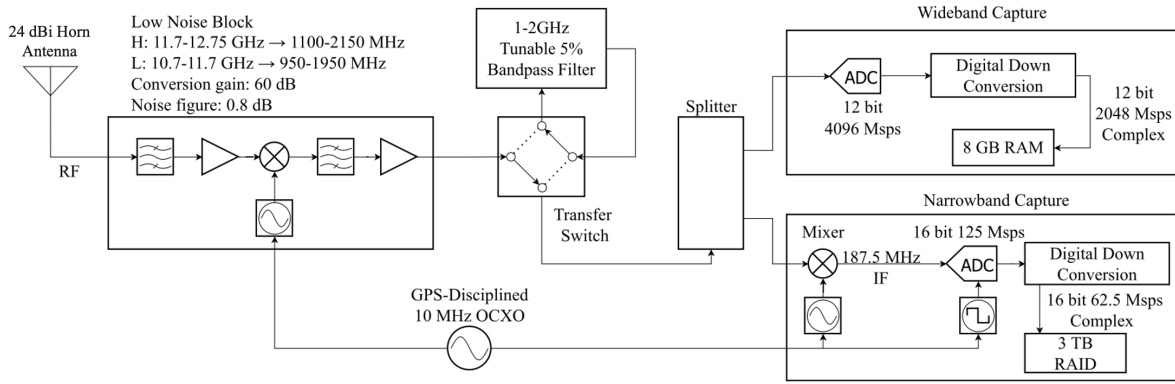


Fig. 5: Block diagram of the capture equipment used in this study. There are two main capture modes: narrowband and wideband. While the former can capture minutes-long recordings with 16-bit complex sampling at 62.5 Msp/s, it can only cover a small portion of even a single Starlink channel, a window insufficiently wide for occupancy studies. The wideband mode can provide a live spectrogram view of six Starlink channels; however, it cannot sample data for more than a small fraction of a second at a time.

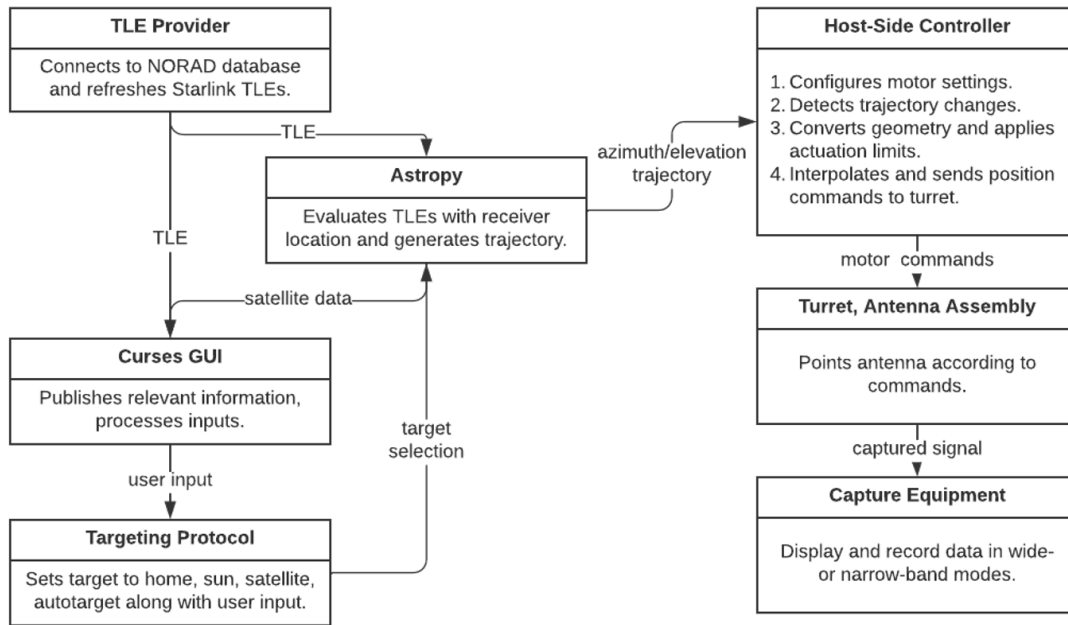


Fig. 6: Block diagram of software used to plan trajectories, track satellites, and actuate the antenna assembly. The four blocks to the left of the arrow labelled "azimuth/elevation trajectory" represents the trajectory manager, complete with the user interface and targeting protocol. The remaining motor controller and physical assembly are represented to the right of the aforementioned arrow.

track and provides the corresponding trajectory to the motor controller.

Upon software start, the motor controller conducts setup routine procedures, such as declaring the required Robot Operating System (ROS) publishers and subscribers for communicating with the pan-tilt mount and setting the PID gains. As the program runs and with each trajectory received, the motor controller processes the new data, translating azimuth-elevation pointing commands to pan-tilt motor commands based upon the known turret geometry. At every timestep, the controller linearly interpolates the motor command time history to the current time before instructing hardware to execute the command.

## V. SATELLITE TRACKING ALGORITHM

We developed the autotargeting algorithm described in Algorithm 1 to: (1) construct an initial upper limit for the number of satellites transmitting to a single service cell with assigned beams and (2) establish a simple baseline heuristic method that

```

0
1 ID | Az | El | Heur
2 -----+-----+-----+-----
3 STARLINK-5940 | 134.16 | 67.61 | 13057.69
4 STARLINK-2655 | 262.05 | 64.49 | 11250.14
5 STARLINK-6120 | 44.93 | 58.63 | 12992.69
6 STARLINK-4180 | 314.64 | 54.44 | 12530.87
7 STARLINK-1630 | 88.70 | 52.00 | 10053.80
8 STARLINK-3811 | 204.02 | 50.65 | 8988.91
9 STARLINK-5104 | 215.97 | 49.14 | 9635.09
10 STARLINK-5264 | 125.68 | 47.71 | 7714.45
11 STARLINK-4796 | 54.53 | 40.63 | 11844.33
12 STARLINK-3319 | 277.92 | 40.52 | 8603.53
13 STARLINK-1086 | 340.42 | 39.57 | 5963.53
14 STARLINK-6081 | 127.60 | 36.08 | 4961.71
15 STARLINK-2582 | 327.68 | 34.98 | 12102.19
16 STARLINK-5106 | 312.19 | 34.83 | 5120.15
17 STARLINK-1692 | 194.88 | 34.72 | 6428.09
18 STARLINK-1923 | 151.74 | 33.98 | 4896.35
19 STARLINK-3520 | 181.18 | 33.11 | 7961.25
20 STARLINK-5806 | 340.44 | 31.69 | 7138.24
21 STARLINK-4148 | 222.62 | 31.66 | 2654.08
22 STARLINK-1878 | 39.42 | 30.66 | 12695.01
23
24 Receiver location (lat/lon):
25 30.283620 | -97.739560
26
27 Current time (UTC):
28 2023-08-28 19:08:08.612541+00:00
29 Current time (local):
30 2023-08-28 14:08:08.612539
31 Countdown to possible satellite handoff:
32 3.4
33 Sun position (az/el):
34 203.92527599808065, 67.67502600405761
35
36 Currently targeting: satellite
37 Autotarget: True
38 Commanded Turret Position: [147.0210240556727, 30.468147556630683]
39 Turret Trim: [0.0, 0.0]
40

```

Fig. 7: A screenshot of the Python curses TUI. A table of overhead Starlink satellites ordered by decreasing elevation occupies much of this interface. Below, important environmental and targeting data is displayed to the user, including current time, IP-geolocated position, and current azimuth-elevation command.

identifies satellites with assigned beams. It should be noted that as the capture hardware currently limits our data processing method to a live wideband spectrogram rather than cross-correlation-based detection, investigations of side beam occupancy are yet unviable. Nonetheless, power-based channel occupancy investigations of assigned beams are still viable.

---

**Algorithm 1** Autotargeting algorithm for assigned beam exploration.

---

```

m ← 3
while true do
  t := TIMENOW
  cf := floor(TOGPSSECONDS(t)/15)
  S := GETSATELLITES(t)
  i := 1
  foreach s ∈ S do
    H[i] ← CalcHeur(s)
    i ← i + 1
  sorted := SORT(H, decreasing)
  T := S[sorted]
  j := 0
  while j < m do
    TRACKSATELLITE(T[j])
    WAIT(15/m)

```

---

To reiterate, the autotargeting algorithm explores the number of simultaneously assigned beams available to a receiver. Note, however, that simultaneous observation of multiple satellites using a narrow-beam antenna is generally unfeasible. The algorithm

mitigates this shortcoming by leveraging the FAI as introduced in Section III-A. From the observation that no alterations in beam or channel assignments occur during the same FAI, we conclude that a single detection of a satellite assigned beam assures the assignment of the satellite for the duration of the entire FAI. Consequently, the total count of individual satellites with assigned beams observed is a sufficient substitute for the number of concurrently assigned beams. This, in turn, motivates us to maximize the number of satellites visited within a single 15-second interval.

The maximum number of satellites we can visit within the same FAI is limited by the dwell and switch times. If real-time matched filtering were possible, then we could assume only a short dwell time ( $< 1$  s) is required to determine the presence of an assigned beam. Yet, given that the observational methods involved human interpretation of a live spectrogram, we require a much more substantial dwell time of several seconds to either validate or dismiss channel occupancy. This imposed a limitation on the number of unique satellite observations per FAI. When considering three satellites for observation per FAI, the allotted combined dwell and switching time becomes 5 seconds, below which we would expect the rate of detection errors to rise substantially. Consequently, we set the number of satellites visited for a given FAI  $m = 3$  for this study.

Observations informed us that satellites with high signal strength and frequent transmissions tended to occupy elevated positions and exhibited prolonged presences in the sky, as opposed to satellites that barely skim our field of view at low, near-horizon elevations. Accordingly, we adopted a basic heuristic based on the integration of elevation versus time during the current FAI.

Let  $\mathcal{I}$  be the set of all SVs above the horizon, and  $\mathcal{J}$  be all the visited SVs in the  $k$ th FAI. Then, let  $\theta_i(t)$  represent the elevation time history of the  $i$ th satellite and  $t_k$  the start time of the  $k$ th FAI. We then used the simple heuristic in (1) to determine which three satellites to observe during each FAI.

$$i_{\text{next}} = \operatorname{argmax}_{i \in \mathcal{I} \setminus \mathcal{J}} \int_{t_k}^{t_{k+1}} \theta_i(t) dt \quad (1)$$

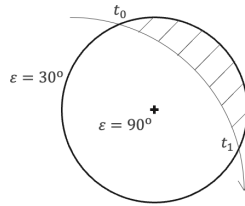


Fig. 8: Diagram of satellite track crossing the sky, where the ribbed area represents the heuristic used to determine satellite tracking patterns.

## VI. RESULTS

Two sets of results were produced using the narrowband and wideband capture modes. First, we validated the tracking of a Starlink satellite despite comprehensive hardware and software updates. This confirmation was achieved via a cross ambiguity function (CAF) of known Starlink signal portions, the PSS and SSS, against a captured signal. Subsequently, we investigated the number of concurrently assigned beams within a given FAI.

$$S(f, k) = \sum_n r(n+k)c^*(n)e^{-2i\pi f\Delta t} \quad (2)$$

(2) shows the cross-correlation of the received signal  $r(n)$  delayed by  $k$  samples against a local replica  $c(n)$ .  $f$  is the Doppler frequency in Hz, and  $\Delta t$  represents the sample interval. As  $f$  approaches the true Doppler experienced and  $k$  results in a TOA measurement close to the true TOA, the cross-correlation between  $r$  and  $c$  constructively interfere, giving rise to a higher result  $S$ . After repetition across a wide search grid of varying Dopplers and TOAs, we can construct a CAF as shown in Fig. 9. Given that the local replica used was the time-concatenated PSS and SSS, the existence of a significant relative peak in the CAF proves successful acquisition of a Starlink satellite.

To investigate the number of concurrently assigned beams and to measure the viability of our heuristic  $H$ , the turret assembly was run autonomously using Algorithm `alg:autotarget` for 30 minutes, or the duration of 120 FAIs. For each of these 120 FAIs, the number of satellites with assigned beams was counted, up to the three visited per FAI. Figs. 10 and 11 show example spectrograms at moments with full and absent assigned beam occupancy, respectively. Fig 12 is a bar chart showing the distribution of concurrent assigned beams per FAI.

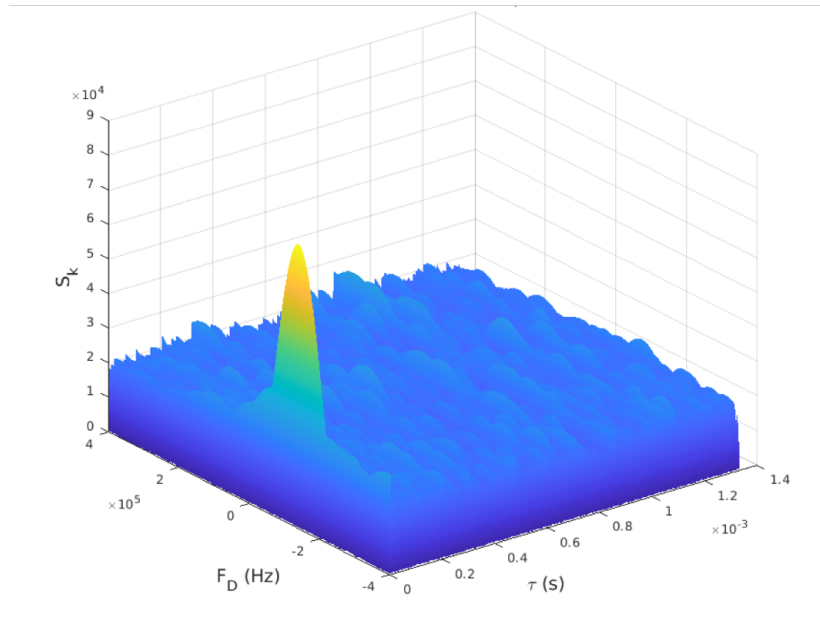


Fig. 9: Cross-ambiguity function results. The peak in cross-correlation at  $F_D \approx -10$  kHz and  $\tau \approx 0.05$  s proves successful capture of a Starlink signal.

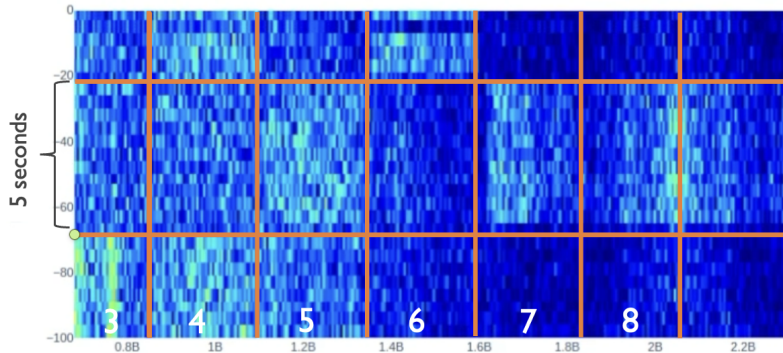


Fig. 10: Example of an active portion of a spectrogram. Six Starlink channels can be seen, from channel 3 through channel 8. The horizontal lines indicate the points at which the autotargeting algorithm changed satellites. This freeze frame shows a recorded observation of three unique satellites concurrently transmitting assigned beams across six channels.

Aggregated, the heuristic was successful in detecting at least one satellite per FAI in 94% of the cases, at least two satellites per FAI in 55% of cases, and all three guesses were successful in 9% of cases. This not only confirms the basic viability of the integrated elevation heuristic upon which more work can be done, but also shows that the potential number of main beams per FAI is at least three.

## VII. DISCUSSION

In this study, a new set of capture equipment was designed, assembled, and tested to pursue a set of open questions whose answers will enable efficient operation of an opportunistic LEO PNT system focused on Starlink broadband transmissions. Briefly restating these open questions, we wish to find: (1) the number of unique SVs a user could possibly use for TOA measurement, (2) a simple pattern to predict assignment triads, and (3) a range of absolute received power into a hemispherical antenna from an assigned or side beam. This section will discuss the degree to which the current results have already answered these questions, and the next steps we are pursuing to fully address them.

With regards to the number of unique SVs from whose transmissions TOA measurements can be made, we confirmed the current upper bound to be three unique SVs transmitting assigned beams. With more exploration, we expect the number of usable assigned to rise, as well as the additional inclusion of the number of usable side beams.

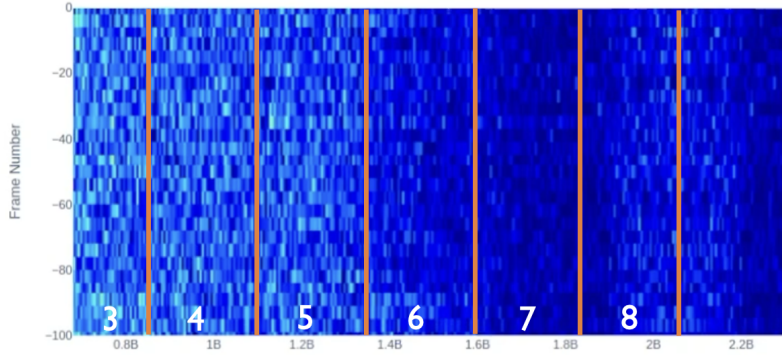


Fig. 11: Example of a spectrogram with no activity. It should be noted that the power is not uniform across the entire 1 GHz bandwidth, which can be partially attributed the antenna gain pattern.

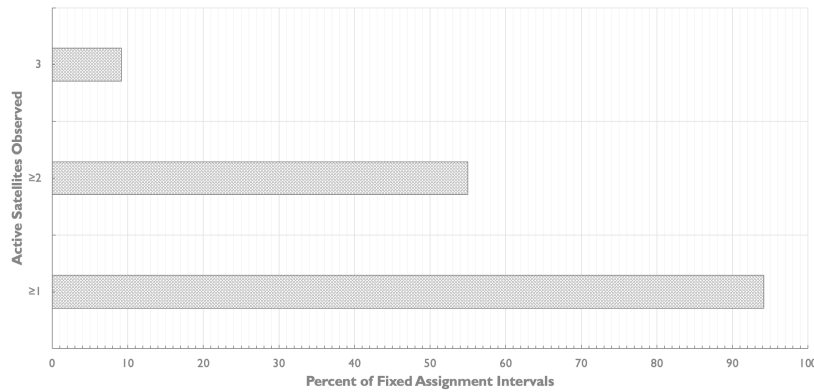


Fig. 12: Bar chart indicating the number of concurrent assigned beams observed per FAI, up to three.

We introduced a simple heuristic to help predict assignment triads per FAI. It acquires at least one assignment triad per FAI for 94% of FAIs. It should be noted, however, that observations were made in a populated urban area where demand is possibly higher than average. Users in areas with lower demand should expect differences in this measurement. Nonetheless, this heuristic provides the basis for further development.

While results for assigned and side beam power estimation have not yet been completed, work is underway. Using pyramidal feedhorn gain estimation techniques such as those presented in [Maybell and Simon, 1993], [Jull, 1973], we can use known parameters of the capture system, Starlink communications system, and signals aggregated over a sufficient number of captures to estimate the expected power per unit area. This figure will allow us to determine if the required SNR is available to support wide beam capture for simultaneous acquisition of several SVs.

In terms of hardware and software development, the next priority is to use a live matched filter against the known portion of the Starlink signal in the control loop, from which we expect a reduction in required dwell time to determine transmission presence. This, in turn, should raise the number of SV visits per FAI several times, with benefits for the exploration of the former two open questions introduced.

## ACKNOWLEDGMENTS

Research was sponsored by the U.S. Department of Transportation (USDOT) under the University Transportation Center (UTC) Program (CARMEN+), and by affiliates of the 6G@UT center within the Wireless Networking and Communications Group at The University of Texas at Austin.

## REFERENCES

- [Blázquez-García et al., ] Blázquez-García, R., Cristallini, D., Ummenhofer, M., Seidel, V., Heckenbach, J., and O'Hagan, D. Capabilities and challenges of passive radar systems based on broadband low-earth orbit communication satellites. *IET Radar, Sonar & Navigation*, n/a(n/a).
- [Dolman, 2012] Dolman, E. C. (2012). New frontiers, old realities. *Strategic Studies Quarterly*, 6(1):78–96.
- [EverythingRF, 2023] EverythingRF (2023). 1000XDF. <https://www.everythingrf.com/products/low-noise-blocks/norsat/698-512-1000xdf>.
- [Humphreys, 2017] Humphreys, T. E. (2017). Interference. In *Springer Handbook of Global Navigation Satellite Systems*, pages 469–503. Springer International Publishing.
- [Humphreys et al., 2023] Humphreys, T. E., Iannucci, P. A., Komodromos, Z. M., and Graff, A. M. (2023). Signal structure of the Starlink Ku-band downlink. *IEEE Transactions on Aerospace and Electronic Systems*, pages 1–16.
- [Iannucci and Humphreys, 2022] Iannucci, P. A. and Humphreys, T. E. (2022). Fused low-earth-orbit GNSS. *IEEE Transactions on Aerospace and Electronic Systems*, pages 1–1.
- [Jull, 1973] Jull, E. (1973). Errors in the predicted gain of pyramidal horns. *IEEE Transactions on Antennas and Propagation*, 21(1):25–31.
- [Komodromos et al., 2023] Komodromos, Z. M., Qin, W., and Humphreys, T. E. (2023). Signal simulator for Starlink Ku-Band downlink. In *Proceedings of the ION GNSS+ Meeting*.
- [Maybell and Simon, 1993] Maybell, M. and Simon, P. (1993). Pyramidal horn gain calculation with improved accuracy. *IEEE Transactions on Antennas and Propagation*, 41(7):884–889.
- [Nardin et al., 2020] Nardin, A., DAVIS, F., and Fraire, J. A. (2020). Empowering the tracking performance of LEO PNT by means of meta-signals. In *2020 IEEE International Conference on Wireless for Space and Extreme Environments (WiSEE)*, pages 153–158. IEEE.
- [Neinavaie et al., 2021] Neinavaie, M., Khalife, J., and Kassas, Z. M. (2021). Exploiting Starlink signals for navigation: First results. In *Proceedings of the ION GNSS+ Meeting*, pages 2766–2773, St. Louis, Missouri.
- [Neinavaie et al., 2022] Neinavaie, M., Khalife, J., and Kassas, Z. M. (2022). Acquisition, doppler tracking, and positioning with Starlink LEO satellites: First results. *IEEE Transactions on Aerospace and Electronic Systems*, 58(3):2606–2610.
- [NSI-MI, 2023] NSI-MI (2023). Standard gain horns. <https://www.nsi-mi.com/products/antenna-products/standard-gain-horns>.
- [Psiaki, 2021] Psiaki, M. L. (2021). Navigation using carrier Doppler shift from a LEO constellation: TRANSIT on steroids. *Navigation, Journal of the Institute of Navigation*, 68(3):621–641.
- [Robotics, 2023] Robotics, T. (2023). WidowX dual XM430 pan & tilt. <https://www.trossenrobotics.com/widowx-x-series-dual-servo-robot-turret.aspx>.
- [Robotis, 2023] Robotis (2023). Dynamixel XM430-W350-R. <https://www.robotis.us/dynamixel-xm430-w350-r/>.
- [SpaceX, 2019] SpaceX (2019). SpaceX non-geostationary satellite system, Technical Parameters. [https://licensing.fcc.gov/myibfs/download.do?attachment\\_key=1877844](https://licensing.fcc.gov/myibfs/download.do?attachment_key=1877844). SAT-MOD-20190830-00087.
- [Teng and Wang, 2016] Teng, Y. and Wang, J. (2016). A closed-form formula to calculate geometric dilution of precision (GDOP) for multi-GNSS constellations. *GPS Solutions*, 20(3):331–339.
- [Vallado et al., 2006] Vallado, D., Crawford, P., Hujsak, R., and Kelso, T. (2006). Revisiting spacetrack report # 3. In *AIAA/AAS Astrodynamics Specialist Conference and Exhibit*, page 6753.
- [Yang and Soloviev, 2023] Yang, C. and Soloviev, A. (2023). Starlink Doppler and Doppler rate estimation via coherent combining of multiple tones for opportunistic positioning. In *2023 IEEE/ION Position, Location and Navigation Symposium (PLANS)*, pages 1143–1153. IEEE.